Electronic Supplementary Material (ESI) for Nanoscale.

SUPPORTING INFORMATION

Digital Counting of Nucleic Acid Targets using Solid-State Nanopores

*Eric Beamish, Vincent Tabard-Cossa, Michel Godin**
University of Ottawa – Department of Physics

***michel.godin@uottawa.ca**

Table of contents

Section S1. Molecular assembly.

Sketches of the structures used in this this work are shown in Figure S1, roughly to scale with respect to one another. The corresponding sequences are shown in Table S1, which is roughly grouped by assembled complex structure. **Scaffold**, **3'-CompA** and **CompB-33mer** oligos are used in both PS- and AC-155, and PS- and AC-141.

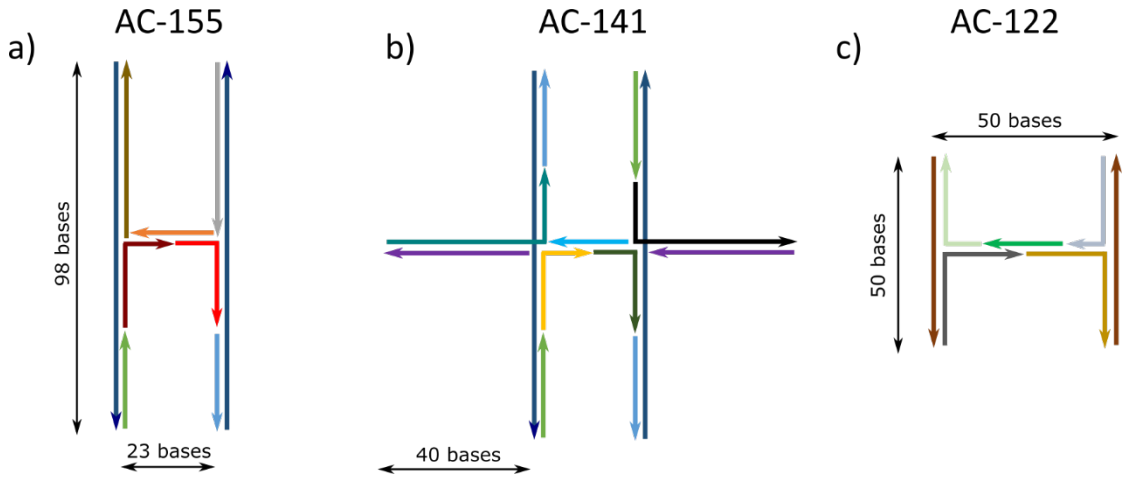

Figure S1. Schematic representations of assembled probe-target complexes. Sketches correspond to targets miRNA-155 or ssDNA-155 (a), ssDNA-141 (b) and ssDNA-122 (c). Arrows representing the oligonucleotides point in the 3' to 5' direction, with the associated sequences in Table S1.

Table S1. Oligonucleotide sequences. Sequences are grouped by target and associated probe structures, colour-coded to match Figure S1. Where appropriate, some sequences were shared between structures in Figure S1a and S1b. RNA is denoted with lowercase 'r' before each base.

Name	Sequence (5'-3')	Length
miRNA-155	rUrUrArArUrGrCrUrArArUrCrGrUrGrArUrArGrGrGrGrU	40
ssDNA-155	TTAATGCTAATCGTGATAGGGGT	23
Scaffold	GGTGTGACTTGAATTTGCGGTCCTAAGTTGGTTCGTAATTGTGGTCATCGTGGCGTACCATATACCGCTTGTTGTATTCTAACACTGCATCTCATACG	98
5'-compA	ACAATTACGAACCAACTTAGGACCGCAAATTCAAGTCACACC	42
3'-compA	CGTATGAGATGCAGTGTTAGAATACAACAAGC	32
Overhang-A-155	GGTATATGGTACGCCACGATGACCTACCCCTATCAC	36
Comp-B-33mer	AACCAACTTAGGACCGCAAATTCAAGTCACACC	33
Overhang-B-155	GATTAGCATTAATCCACGATGACCACAATTACG	33
Comp-B-45mer	CGTATGAGATGCAGTGTTAGAATACAACAAGCGGTATATGGTACG	45
ssDNA-141	TAACACTGTCTGGTAAAGATGG	22
Overhang-A-141	GGTATATGGTACGCCATCCATCTTTACC	28
Overhang-B-141	AGACAGTGTTATCGATGACCACAATTACG	29
Branch-comp	CGTGCACATCGTCAGCATACGTACGCTACCTCGACCTGCG	40
A-branch	CGCAGGTCGAGGTAGCGTACGTATGCTGACGATGTGCACGTCGATGACCACAATTACG	58
B-branch	GGTATATGGTACGCCATCGCAGGTCGAGGTAGCGTACGTATGCTGACGATGTGCACG	57
ssDNA-122	TGGAGTGTGACAATGGTGTTTG	22
3-A-5'	AAGGACCAGGGAACGTATTTGCCTTGTCTGGGAAATCGT	39
3-AB	ACGATTTCCCAGACAAGGCAAATACCCAACTGGTTGTGGCCTATCGAAAA	50
3-A-3'	TTTTCGATAGGCCACAACCAGTTGGGTTCCCTGGTCCTTCAAACACCATT	50
3-B-5'	GTCACACTCCAAAGGACCAGGGAACGTATTTGCCTTGTCTGGGAAATCGT	50
3-B-3'	TTTTCGATAGGCCACAACCAGTTGGGTTCCCTGGTCCTT	39

Section S2. Gel Characterization.

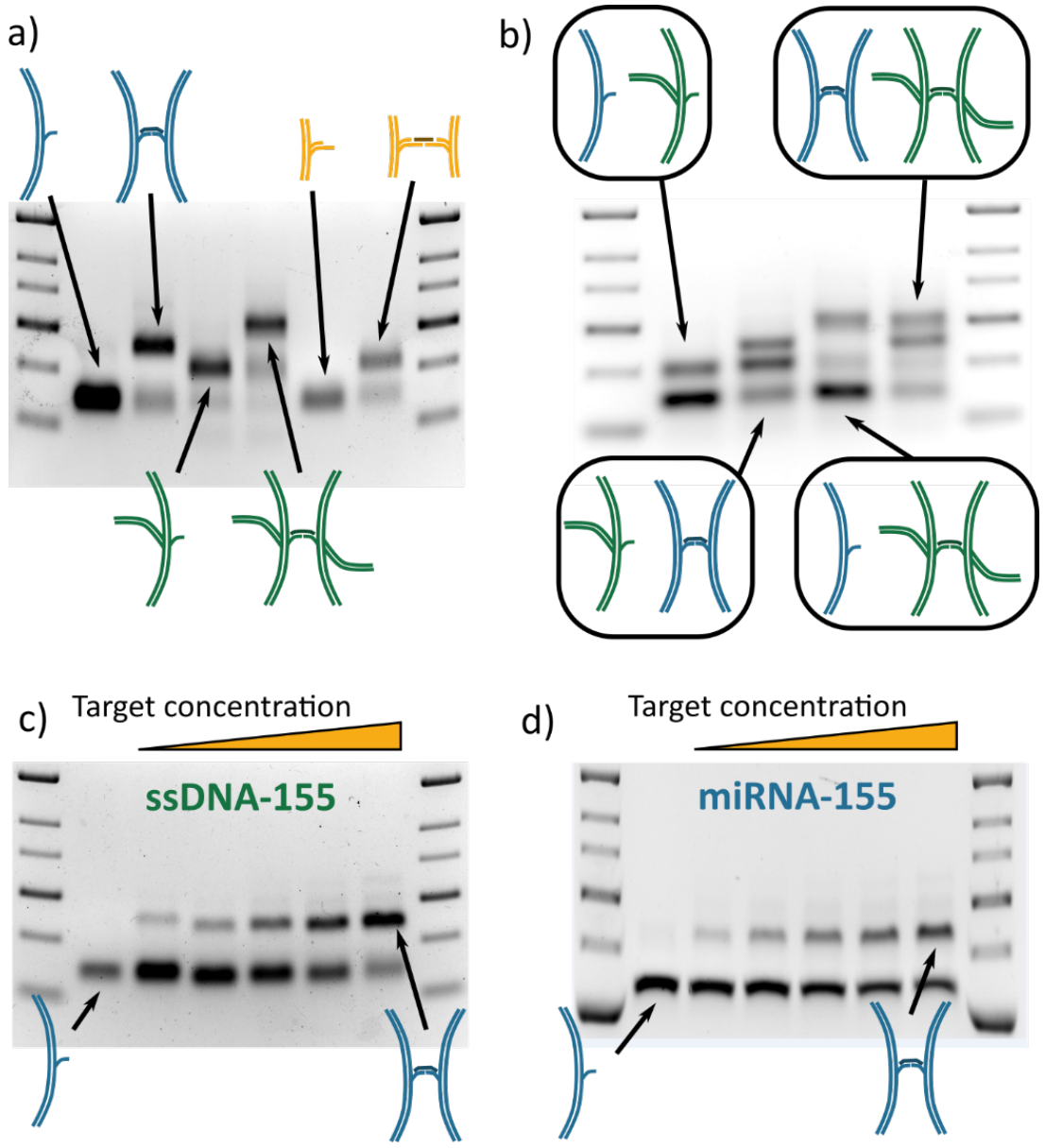

Figure S2. Gel characterization of assembled molecules. a) Probe sets and assembled molecules for the experiments shown in Figure 1. b) Sample mixtures for 2-plex target detection shown in Figure 2. Dose response assays in which increasing concentrations of ssDNA-155 (c) and miRNA-155 hybridize to the same probe set (PS-155). Figures 3 and 4 of the manuscript use the sample mixtures in (d). All assembled molecules were characterized by 2 % agarose gel electrophoresis with outer lanes containing a 1 kbp ladder. Relative intensities within each lane were quantified using GelBandFitter[1] as described elsewhere.[2]

In addition to the gels shown in Figure S3, the dose response of miRNA-155 hybridization to linear probe sets was tested over different concentration ranges. Figure S3 shows an example reaction where molar excesses of target were added to a fixed concentration of each probe. After reaching a maximum reaction yield of ~50%, a decline in assembled complexes is observed, as conjugation is prevented when binding sites become saturated with the miRNA target.

While a slightly higher yield was observed for a molar ratio of 1.5 as compared to the expected ratio of 1 for maximum yield, we expect that this was due to a higher degree of adsorption of miRNA to tube walls relative to that of the probes upon storage or incubation, resulting in fewer target molecules that were accessible for reaction than expected based on spectrophotometer measurements prior to dilution to experimental concentrations. Nanopore results of this sample (molar ratio of 1.5) did not show a statistically significant difference from the molar ratio of 1 shown in Figure 3 (data shown in Supporting Information Section S5).

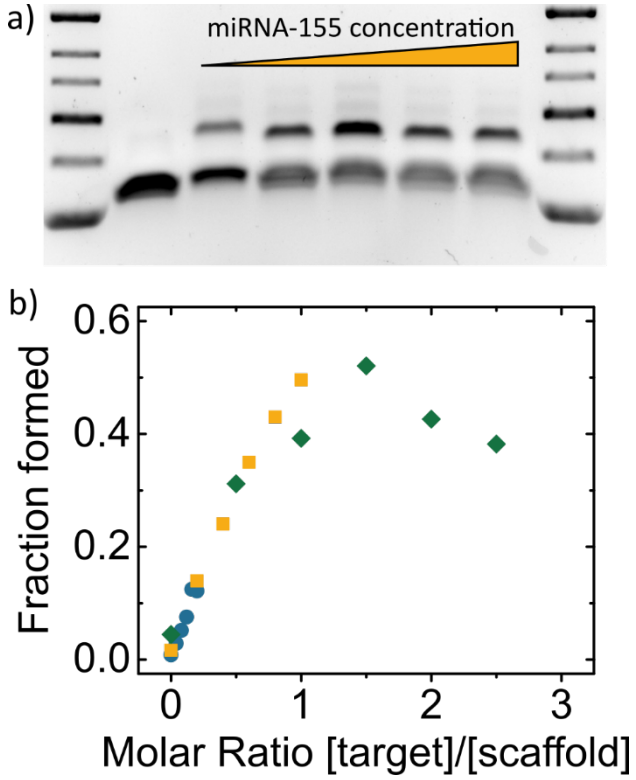

Figure S3. Effects of high miRNA concentration. a) Agarose gel characterisation of a reaction in which target concentrations exceeded those of probe sets. The reaction yield of each mixture in (a) is shown as green diamonds in (b), where two other reaction sets spanning different concentration ranges are also characterised. Yellow squares correspond to the gel shown in Figure S2d and the nanopore translocation data presented in Figures 3 and 4 of the manuscript.

Section S3. Translocation characteristics of 100 bp dsDNA fragments, PS-155 and AC-155.

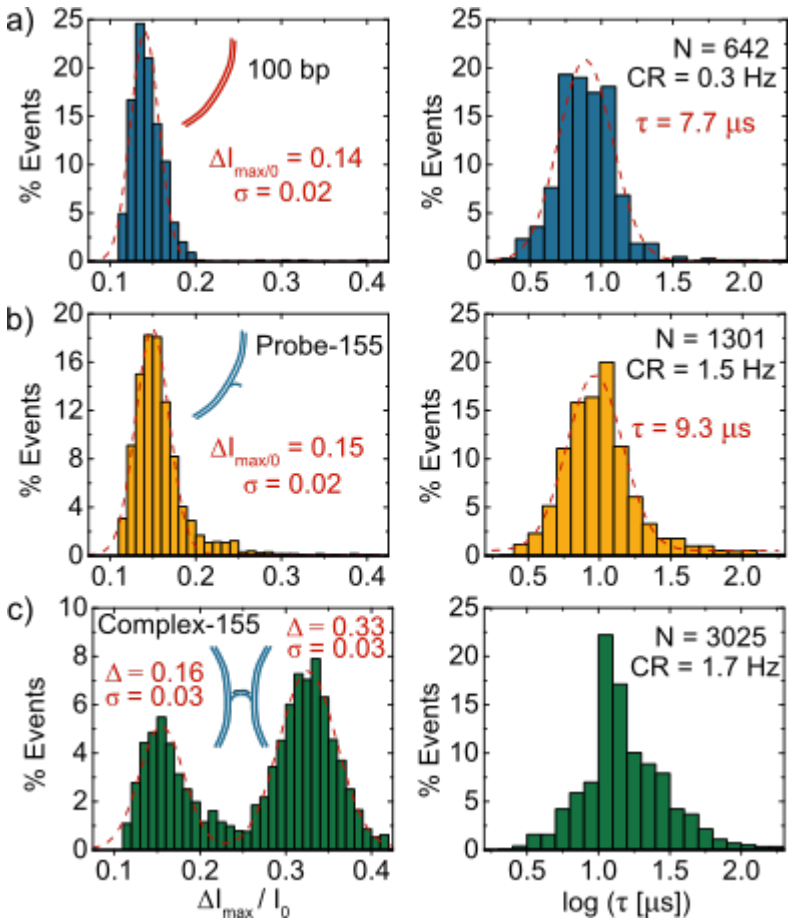

Figure S4. Histograms of ΔI_{max} relative to the open pore current I_0 and log(τ) for a) 100 bp fragments, b) PS-155, and AC-155 hybridized with ssDNA-155. Dashed red lines are Gaussian fits with indicated peak locations and standard deviations. The log(τ) histogram for the assembled complex was not fit due to the bimodal distribution of translocation events, as seen in Figure 1 of the manuscript. CR refers to the capture rate of each species for particular characterisation experiments.

Section S4. Preliminary 3-plex experiments.

While Figure 2 shows the successful simultaneous detection of two different ssDNA targets, we also performed experiments in which all three probe sets examined were sensed simultaneously with the same nanopore. In this case, all samples from Figure 1 were prepared separately and mixed in equimolar ratios for a final total probe set concentration of 55 nM for addition to the nanopore system (i.e. each probe of a set was mixed in equimolar ratios with the indicated target, and respective mixtures were combined in equimolar molar ratios of probes – each approximately 18 nM during sensing). Control samples were prepared at similar concentrations, but without the target.

Figure S6 shows histograms of the maximum blockage depth observed for three 3-plex experiments. Schematic insets show which species were added in each example, with arrows indicating the corresponding peaks (or lack of corresponding peaks) that can be used to identify which samples were present. Given the amount of unreacted probe sets, distinguishing the small 50-base branched scaffold (Complex-122) was not possible in these reaction mixtures. However, the two larger assembled complexes could be identified by the presence or absence of peaks at deeper blockage depths. Such experiments would likely benefit from machine learning algorithms for analysis.[3]

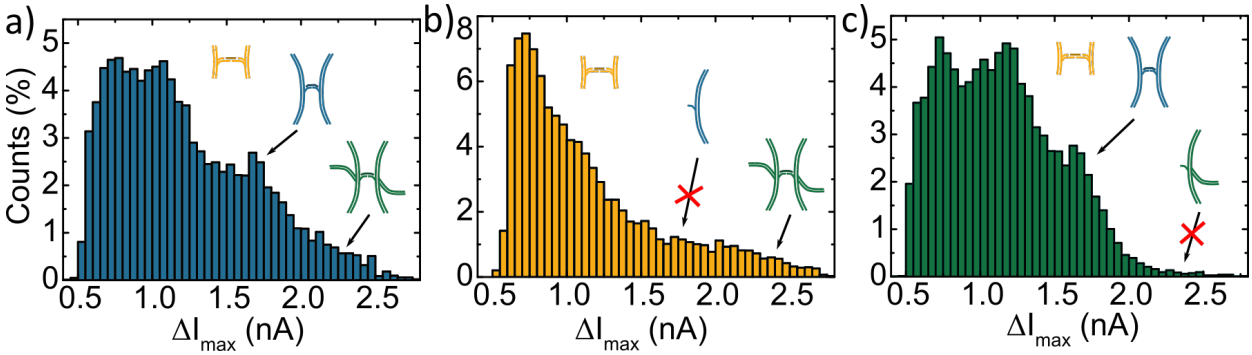

Figure S5. Preliminary 3-plex target detection experiments at 100 mV. a) The assembled complex associated with targets ssDNA-155 and ssDNA-141 yields a peak at deeper blockage depths (ΔI_{max} > 1.5 nA) to identify ssDNA-155 and ssDNA-141. The presence or absence of these peaks is also resolvable in samples where only one of those targets is in the sample mixture (b-c). The complex associated with ssDNA-122 is at present indistinguishable due to a high degree of unreacted molecules corresponding to all samples.

Section S5. Statistical confidence of miRNA detection.

While Figure 4.4 shows 95 % confidence intervals around the mean for differentiating samples of increasing miRNA concentration, we also performed similar analysis using a 99 % confidence interval. Figure S7 shows a plot similar to Figure 4, but with lightly shaded regions around each mean corresponding to this stricter criterion. The number of events required to differentiate neighbouring concentrations is shown as dashed lines with two asterisks. As shown in Figure 4, all samples were distinguishable in fewer than 3000 events, with the exception of the target ratios of 1.5 and 1.0.

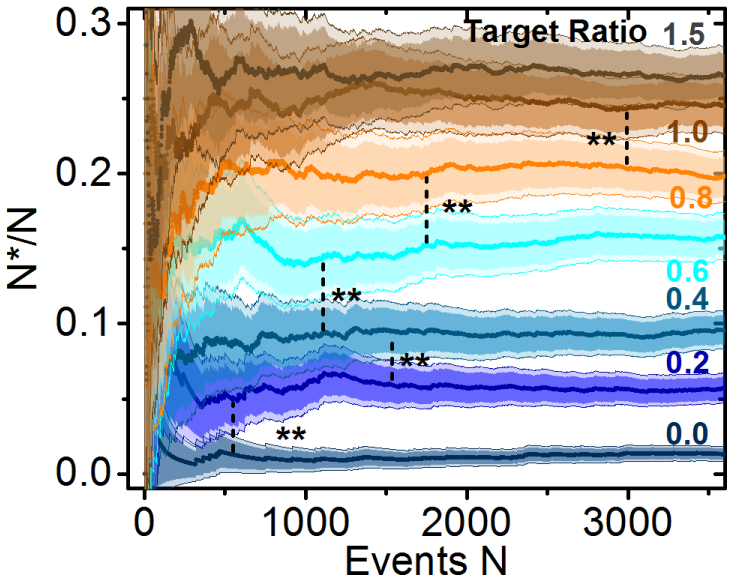

Figure S6. Statistical analysis of complex detection with two confidence intervals. Similar to Figure 4 of the manuscript, the mean number of assembled complexes detected as a function of the cumulative number of events is shown with dark shaded regions representing a 95% confidence interval. Lightly shaded regions correspond to a 99% confidence interval, with dashed lines indicating where samples containing similar miRNA to probe ratios were resolved with this stricter criterion. Calculations were performed as previously described.[4]

Section S6. ssDNA-155 vs. miRNA-155 with PS-155.

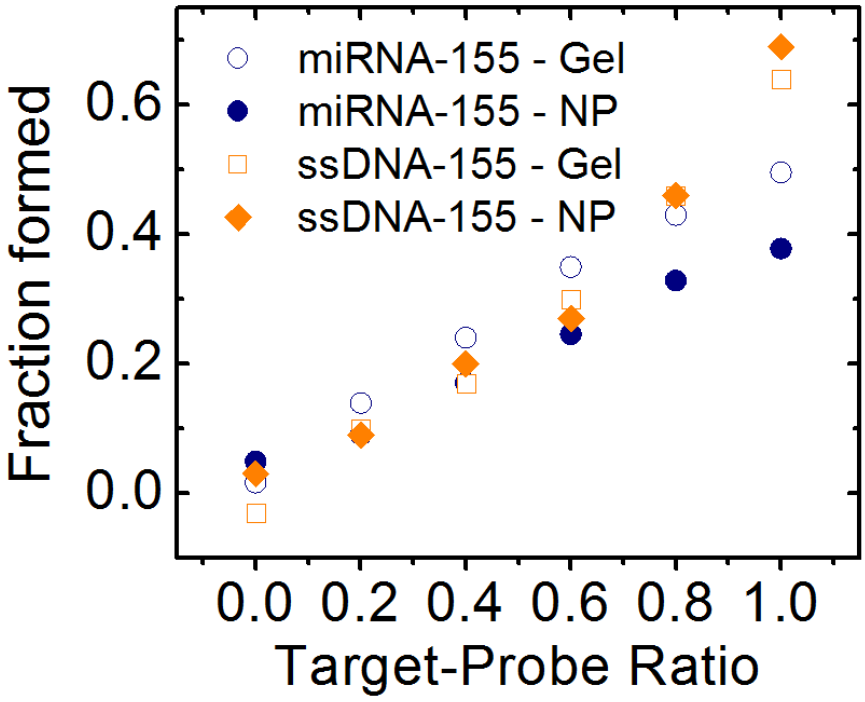

Figure S7. Reaction yields of ssDNA-155 and miRNA-155 with PS-155 as characterised by 2% gel electrophoresis and solid-state nanopores. The gel data corresponds to that of Figure S2, while the miRNA-155 – NP data is that shown in Figure 3d of the manuscript.

Section S7. Ionic current traces.

Figure S8 shows ionic current traces for each sample as recorded by different nanopores between 7-10 nm in diameter. For probe sets (the four columns on the left of Figure S8), the first 10 events that were recorded are shown. For assembled complexes, the first 10 events are shown that met a maximum deviation in ionic current, as described in the manuscript. We note that the probe sets corresponding to light blue and light purple are identical samples (PS-155), and yet exhibit slightly different translocation characteristics due to pore-to-pore variability. Despite this, the maximum deviation in ionic current in each event provides a good metric for determining whether a complex has formed, due to the relative counts-based approach to target quantification described herein, where an internal standard is always present in the form of unbound probes.

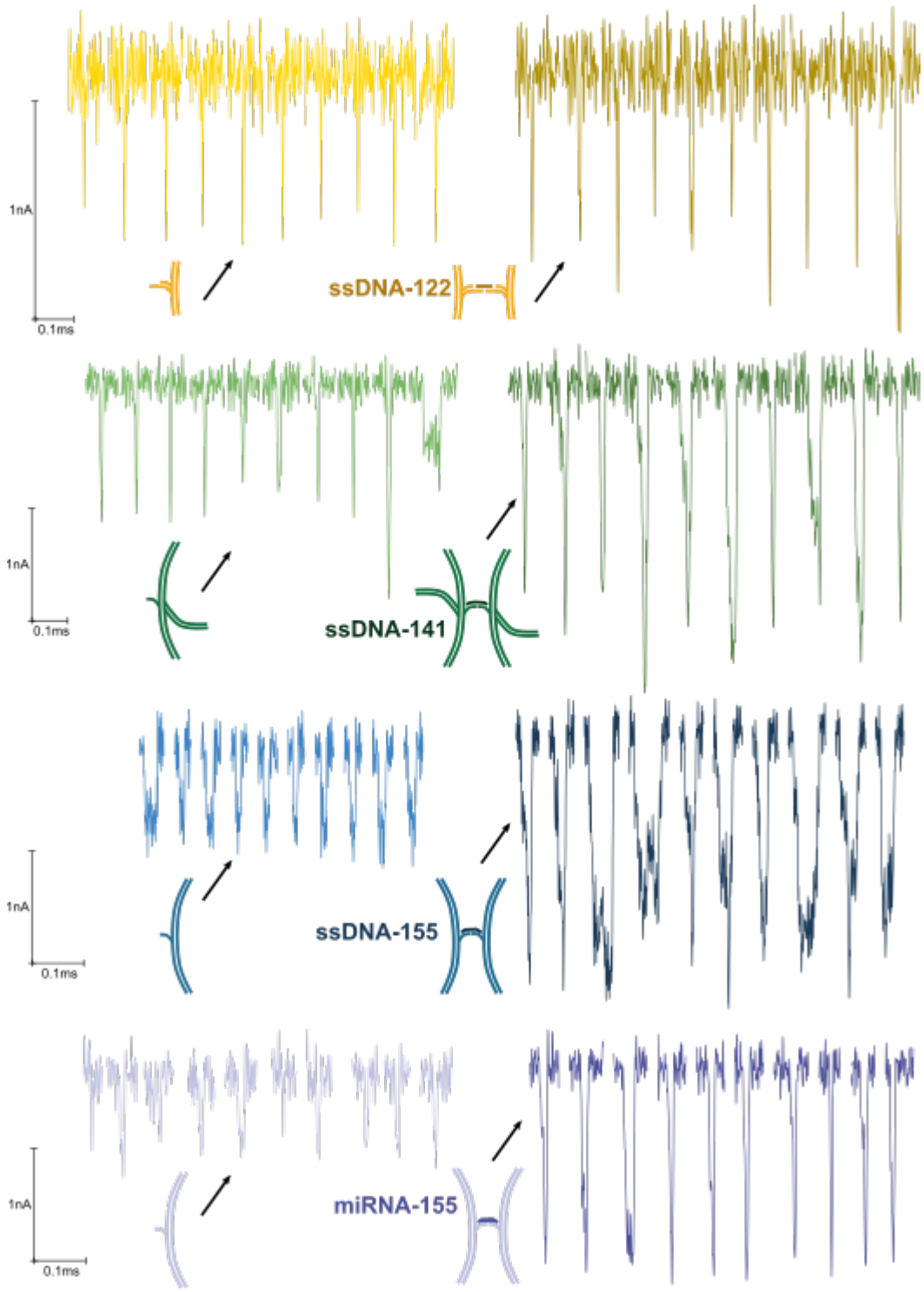

Figure S8. Representative ionic current traces. The first ten events recorded for each sample at 100 mV are shown for probes sets (left), while the first ten events that had a sufficient maximum deviation in ionic current to be identified as an assembled complex are shown for samples containing target (right).

References

1 M. I. Mitov, M. L. Greaser and K. S. Campbell, *Electrophoresis*, 2009, **30**, 848–851.
2 E. Beamish, V. Tabard-Cossa and M. Godin, *ACS Sens.*, 2019, **4**, 2458–2464.
3 K. Misiunas, N. Ermann and U. F. Keyser, *Nano Lett.*, 2018, **18**, 4040–4045.
4 T. J. Morin, T. Shropshire, X. Liu, K. Briggs, C. Huynh, V. Tabard-Cossa, H. Wang and W. B. Dunbar, *PLOS ONE*, 2016, **11**, e0154426.